Formation and ordering of Ge nanocrystals on SiO_2

A. Karmous, I. Berbezier, and A. Ronda
L2MP UMR CNRS 6137, Polytech'Marseille, Technopole de Château Gombert, 13451 Marseille Cedex 20, France
(Received 29 April 2005; revised manuscript received 23 November 2005; published 21 February 2006)

This paper describes the mechanisms of formation and ordering of Ge nanocrystals on a pre-patterned silica layer. In the first part, we investigate the nucleation and growth of Ge nanocrystals during thermal annealing of an amorphous Ge layer. In particular, morphological evolution of nanocrystals with different experimental parameters is analyzed. We show that nanocrystals exhibit a pseudoequilibrium shape independent on annealing conditions; their size and density being only controlled by the deposited thickness of the amorphous layer. This behavior is explained by a nucleus density saturation due to the presence of exclusion zones around critical nuclei. In the second part, we evidence a very nice ordering of Ge nanocrystals inside the focused ion beam (FIB) patterns of a thin silica layer. Preferential nucleation of nanocrystals inside the holes is mainly explained by energetic arguments. In particular, we find that surface free energy is dramatically reduced when nanocrystals are located inside the holes instead of on the flat top surface between the holes. From a kinetic side, preferential nucleation inside the FIB holes should also be favored due to the lower surface diffusion inside the holes.

DOI: 10.1103/PhysRevB.73.075323 PACS number(s): 81.15.Np, 81.10.Jt, 68.35.−p

I. INTRODUCTION

During the last decades, much effort has been devoted to the study of semiconductor quantum dots for their interest both in fundamental physics and device applications. Due to their reduced dimensions, such nanostructures exhibit unique physical properties based on quantum confinement. Moreover, the controlled fabrication of semiconductor quantum dots remains a key requirement for the development of future nanoelectronic devices such as single electron transistor or nanocrystal (NC) memories. The latter device utilizes a new memory-cell concept[1] based on a floating-dot gate embedded in an oxide layer between the control oxide and the source-drain conduction channel. Until now, most of the studies in this field have been devoted to the fabrication of devices based on self-assembled Si NC[2–4] and on their physical properties.[5–7] In first experiments the formation of Si NC was obtained during the thermal oxidation steps.[8] Other processes such as low energy Si implantation,[9–11] and selective chemical vapor deposition (CVD) on thermal SiO_2,[12] have been successfully developed, allowing one to achieve a high control of tunnel oxide thickness and large NC density. However, these processes are far from the desired reproducibility required for the understanding and modeling of NCs structure and properties.[13–17]

Replacing Si NC by Ge NC is expected to improve the memory characteristics (charging time and retention time) because of the smaller band gap of Ge which induces a valence band offset between the substrate and NC.[18–22] Recently, various self-assembling methods based on the Stranki-Krastanov growth mode of Ge on Si substrate have been attempted in order to create regular two-dimensional (2D) arrays of Ge NCs.[23–27] In this system, the self-assembling process is mainly controlled by the gradient of stress relaxation during epitaxial growth. Such a phenomenon cannot be used when Ge NCs are deposited on an amorphous layer. In the latter case, the random heterogeneous nucleation of Ge NCs induces a lack of lateral ordering. Furthermore, kinetics of NCs nucleation, growth, and coalescence lead to large size nonuniformity[28] which is not fully understood. To our knowledge, these mechanisms have not been extensively studied in the literature.

The aim of this paper is to understand first the kinetics of NCs formation and second the driving forces of NCs ordering. This paper is divided into two parts, first the nucleation and growth of Ge NCs during crystallization of an amorphous Ge layer deposited on SiO_2. In this part, morphology, size, and distribution of NCs are analyzed as a function of annealing time and temperature and deposited thickness. In a second part we use a prepatterned amorphous silica layer with well-controlled and scalable patterns. The driving forces of Ge NCs self-assembling are discussed.

II. EXPERIMENTS

Experiments were performed on thin SiO_2 layers obtained by thermal oxidation of Si(001) substrate. SiO_2 prepatterning was produced by focused ion beam (FIB) milling. A field oxide, 500 nm thick, was first fabricated on all silicon (001) wafers. Using standard optical lithographic techniques and wet chemical SiO_2 etching, $10\times 10\ \mu m^2$ windows were opened in this oxide in order to easily locate the arrays of holes produced by the FIB. The wafers were then oxidized again to form the oxide mask for prepatterning (5 nm thick SiO_2 layer). FIB holes height was always deeper than the mask oxide thickness in order to penetrate in the Si substrate.

Milling investigations were performed with a Focused Ion Beam (FIB) FEI XL200. The FIB instrument is equipped with a gallium liquid metal source primary ion gun. With such a type of field emission gun the minimum spot size is $\sim$10 nm and the brightness is very high. Both features combined with the ion mass and the energy used allow a sharp and fast milling of silicon. The FIB process has been performed using a dual beam system in order to minimize the possible gallium implantation during image grabs required

1098-0121/2006/73(7)/075323(5)/$23.00 ©2006 The American Physical Society

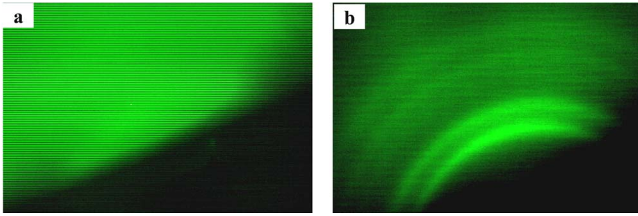

FIG. 1. (Color online) RHEED patterns of a 2 nm thick Ge layer deposited at room temperature: (a) as grown and (b) during the temperature ramp of annealing (at 400 °C).

for target area location. Navigation on the wafer surface is done using scanning electron microscopy (SEM) imaging mode. FIB was used only for milling. Ion source gallium at normal incidence angle with impact energy of 30 keV and 1 pA primary current was used.

After FIB milling, the presence of Ga was detected in the milled areas. A special process was then developed in order to fully restore the substrate cleanliness and to remove Ga below 4×10^{16} cm^{-3}. During this cleaning step, the top part of the FIB patterns is removed with the oxide removal and the bottom part (located in the Si substrate) is slightly enlarged. 3.5 nm thick oxide was subsequently grown and cleaned again. Ge deposition was carried out in a molecular beam epitaxy (MBE) Riber system with a base pressure in the 10^{-11} Torr range. Ge was evaporated from an effusion cell with a deposition rate about 0.017 nm/s.

Amorphous Ge was deposited at room temperature and crystallized during *in situ* thermal annealing at temperatures comprised between 500 and 750 °C. The temperature ramp of the annealing was 50 °C/min. Reflection high energy electron diffraction (RHEED) was used to follow in real time the NCs crystallization. At the end of the annealing, the samples were rapidly cooled at room temperature. Surface morphology was characterized by atomic force microscopy (AFM) operating in non contact mode.

III. RESULTS

During the first series of experiments Ge was deposited on uniformly flat layers of SiO_2 (without FIB patterns). The aim is to describe the crystallization process as a function of annealing conditions and deposited thickness in order to determine the experimental parameters that control the Ge NCs morphological features (shape, size, and density). RHEED pattern evolution was followed in real time during annealing.

After deposition of 2 nm Ge at room temperature, the RHEED pattern of the surface exhibited a diffuse ring pattern representative of an amorphous structure [Fig. 1(a)]. The appearance of well-defined ring patterns, characteristic of crystalline Ge, occurred during the rise in temperature at ~400 °C [Fig. 1(b)]. In such circumstances, it can be deduced that the onset of Ge crystallization occurs at a temperature lower or equal to 400 °C. One can note that diffraction rings indicate a random orientation of the crystallites.

In order to understand the mechanism of NCs formation and evolution, we annealed amorphous Ge layers 2 nm thick at different temperatures (500, 600, 650, and 700 °C) for 30 min. We first checked that the total volume of NCs (estimated from AFM images) is approximately similar to the total volume of the deposited layer in order to confirm the absence of desorption during annealing up to 700 °C. After the annealing, we systematically observed on all the samples the formation of disconnected NCs with a broad size distribution (standard deviation is about 9 nm). The mean NCs density, diameter, and height have been measured by AFM (Table I). The measurements show that all the samples exhibit NCs with identical morphology (aspect ratio $h/\phi\sim0.23$) and density ($D\sim10^{11}/\text{cm}^2$). In a second series of experiments the annealing temperature was fixed at 600 °C and the annealing time was varied from 5 to 10, 20, and 30 min. The NCs morphology and density measured were similar whatever was the annealing time. Moreover, NCs exhibited aspect ratio and density similar to those obtained in the previous set of experiments.

TABLE I. Mean NCs density, diameter, and height measured on AFM images of Ge NCs formed by annealing of 2 nm amorphous Ge for 30 min at 500, 600, 650, and 700 °C.

Annealing temperature	500 °C	600 °C	650 °C	700 °C
Mean NCs density D ($\times10^{10}$ cm^{-2})	10	12.5	11.2	10
Mean diameter ϕ (nm)	28	25	27	27
Mean height h (nm)	6.5	6	6	6.5

Consequently, NCs size and density are independent on annealing parameters (temperature and time) in the experimental conditions investigated here. It can then be concluded that NCs have reached a pseudoequilibrium state characterized by a typical aspect ratio $h/\phi\sim0.23$ and a critical wetting angle $\theta=50°$. Furthermore, it can also be remarked that the NCs height measured by AFM is about three times larger than the deposited thickness. Such a large height cannot be explained by a unique phenomenon of phase transformation from amorphous to crystal. Consequently, the capture of atoms by unwetting and diffusion from extended areas around the critical nuclei should also participate to the nuclei formation.

In the third series of samples the deposited thickness of Ge (h_0) was varied from 1.5 to 5 nm. All the samples were annealed at 700 °C for 30 min. All the samples exhibit highly packed and randomly distributed NCs with a large size distribution. AFM images of the NCs obtained for deposited thickness (h_0) of 5, 3, 2, and 1.5 nm are presented in Figs. 2(a)–2(d). The evolutions of NCs mean density and area with h_0 are plotted in Figs. 2(e) and 2(f). One observes a clear dependence of NCs density (D) and size with h_0. Experimental data can be fitted by $D\propto h_0^{-1}$ and $S_c\propto h_0$ (the NCs radius evolves as $R_{\text{NC}}\propto h_0^{1/2}$). The fit curves are represented as dashed and dot lines, respectively. The opposite evolution of D and S_c is a direct consequence of mass conservation in the case of NCs with equilibrium shape. The linear dependence of the NCs area with the deposited thickness is not explained up to now.

In consequence, we have seen that the mean NCs area ($\bar{S}_c$) and density are only controlled by the deposited thickness

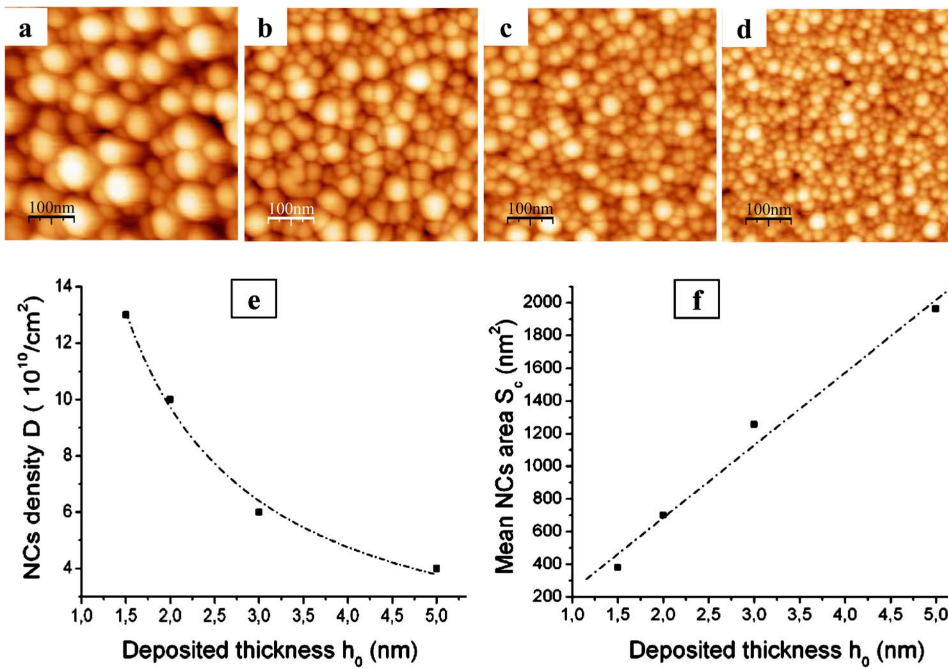

FIG. 2. (Color online) AFM images of samples with different Ge deposited thickness (h_0): (a) $h_0=5$ nm, (b) $h_0=3$ nm, (c) $h_0=2$ nm, and (d) $h_0=1.5$ nm. All these samples were annealed at 700 °C for 30 min. Evolutions of NCs density and mean NCs area with h are presented in (e) and (f), respectively.

(h_0) of the amorphous layer and are independent of the annealing conditions (temperature and time). As a consequence, we can conclude that in all these experiments, a saturation of NCs size and density has been reached. Two processes can be invoked to explain such behavior: a kinetically limited coalescence and a saturation nucleus density caused by exclusion zones around nuclei. The first argument could be explained by a limited surface diffusion. However, such a phenomenon can be ruled out since it would induce a variation of NCs area and density with annealing temperature. Let us develop now the second argument based on thermodynamics. It is reasonable to assume that nucleation occurs just at the interface between the SiO_2 substrate and the amorphous layer of finite thickness (heterogeneous nucleation). The evolution of the growth process cannot be determined from our experimental results, since droplets with pseudoequilibrium shape were obtained whatever were the annealing conditions (temperature and time). Nevertheless, different evolutions could be considered. If the growth process involves the entire layer volume, each nucleus grows through the untransformed volume by converting sites neighboring the surface of the growing nuclei to the new phase.[29] In this case, it is shown that the growth kinetics of 2D nuclei during heterogeneous nucleation is lower than the growth of 3D nuclei involving the entire layer volume. Time variation of the transformed material fraction during heterogeneous 2D nucleation following this model considerably differs from the standard Johnson-Mehl-Avrami (JMA) theory.[30,31]

Alternatively, growth kinetics could follow a two step process involving growth of individual nuclei followed by coalescence of neighboring nuclei.[32] During the first step, nuclei extend in diameter by capturing a large number of neighboring atoms from the amorphous phase. Gradually the surface covered by crystallites increases and when the peripheries of droplet neighbors meet coalescence occurs. As a result, the adatom concentration around the growing crystallites is reduced and the system is locally undersaturated. In these areas (commonly called exclusion areas) nucleation is more or less prohibited. When exclusion zones overlap a saturation of the nucleus density is reached. Then new nuclei do not form and growth of the island stops. The system has reached a pseudoequilibrium state. This explains the invariability of the droplets size/density with annealing conditions in this set of experiments.

In conclusion of these series of experiments, we have shown that it is possible to form highly dense ultrasmall Ge NCs with a shape imposed by the thermodynamics equilibrium and a density/size controlled by the amorphous deposited thickness. This result is in agreement with experimental results on Si/SiO_2 system[33] and Sn/SiO_x.[28]

In the second part of the investigations, Ge has been deposited on FIB patterned silicon oxide in order to determine the driving force of NCs ordering. Figure 3(a) presents the 2D array of FIB nanopatterns after cleaning just before Ge deposition. Patterns consist of nanometer scale holes with mean holes diameter and periodicity of ~25 and ~50 nm, respectively. 2 nm of amorphous Ge was deposited at room

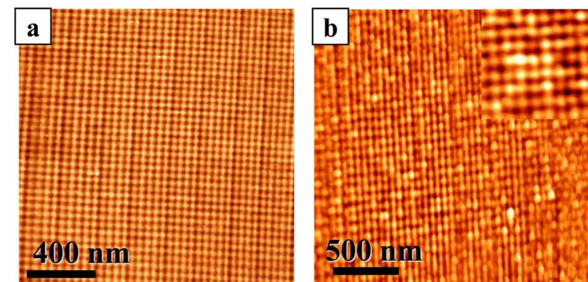

FIG. 3. (Color online) AFM images of FIB patterns on SiO2 substrate: (a) after cleaning. The array period is 50 nm; (b) after room temperature deposition of 2 nm Ge and annealing at 600 °C for 30 min. Islands density is about 4×10^{10} cm^{-2}.

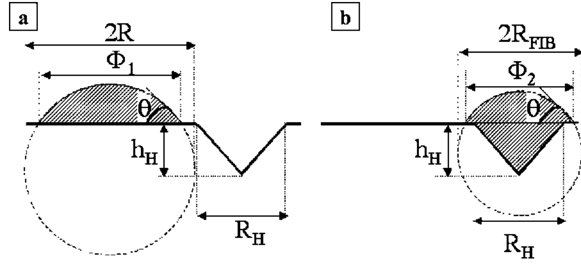

FIG. 4. Schematic view of two NCs of similar volume deposited on (a) a flat surface and (b) a FIB hole.

temperature on the patterned surface and *in situ* annealed at 600 °C for 30 min. The surface after NCs formation is presented in Fig. 3(b). We can see that an efficient ordering has been obtained using FIB patterned substrates and that Ge NCs sizes are homogenized as compared to the size of those obtained on unpatterned areas. Moreover, their density exactly matches the FIB pattern density ($\sim 4.10^{10}/\mathrm{cm}^2$ in the example presented). Nevertheless, AFM image after NCs formation does not allow one to definitely conclude on the nucleation sites location (either inside or in between the FIB holes).

Nucleation of Ge NCs on oxide could be driven by two phenomena, surface diffusion barriers (a lower surface diffusion is expected inside the FIB holes) or surface energy reduction. Regarding the first argument, even if we have seen above that kinetics (and surface diffusion D_s) does not control the evolution of the surface in the $\mathrm{Ge/SiO_2}$ system, NCs nucleation could be sensitive to the surface diffusion inhomogeneity created by the hole patterns. This effect would induce the nucleation of NCs inside the holes.

Regarding the thermodynamics arguments, during the first stage of crystallization the change of free energy of the system can be described by

$$\Delta G = -\frac{V_{a\text{-Ge}}}{v_{a\text{-Ge}}}\Delta\mu + \Sigma_{\mathrm{NC}}$$

with $V_{a-\mathrm{Ge}}$ and $v_{a-\mathrm{Ge}}$ the volume and molecular volume of the amorphous Ge layer respectively, $\Delta\mu$ is the supersaturation and Σ_{NC} accounts for the surface energy and interfacial energy of the NCs.

If we assume that the surface energy is constant (and does not vary with the curvature of the surface) and if we consider two NCs with the same volume, one located on a flat surface [Fig. 4(a)] and the other on a hole [Fig. 4(b)], their difference of surface free energy consists of three terms: $\Delta G = \Delta\sigma_{\mathrm{Ge\text{-}SiO_2}} + \Delta\sigma_{\mathrm{Ge}} + \Delta\sigma_{\mathrm{SiO_2}}$, where

$$\Delta\sigma_{\mathrm{Ge\text{-}SiO_2}} = \pi\sigma_{\mathrm{Ge\text{-}SiO_2}}(\sin^2\theta(R_{\mathrm{FIB}}^2 - R^2) - R_H^2 + R_H\sqrt{R_H^2 + h_H^2})$$

$$\Delta\sigma_{\mathrm{Ge}} = 2\pi\sigma_{\mathrm{Ge}}(1-\cos\theta)(R_{\mathrm{FIB}}^2 - R^2)$$

$$\Delta\sigma_{\mathrm{SiO_2}} = \pi\sigma_{\mathrm{SiO_2}}(\sin^2\theta(R^2 - R_{\mathrm{FIB}}^2) + R_H^2 - R_H\sqrt{R_H^2 + h_H^2}),$$

$\sigma_{\mathrm{Ge\text{-}SiO_2}}$, σ_{Ge}, and $\sigma_{\mathrm{SiO_2}}$ are the Ge-$\mathrm{SiO_2}$ interfacial energy and the Ge and $\mathrm{SiO_2}$ surface energy respectively; that are related by the well-known Dupré expression: $\sigma_{\mathrm{SiO_2}} = \sigma_{\mathrm{Ge\text{-}SiO_2}} + \sigma_{\mathrm{Ge}}\cos\theta$, where θ is the wetting angle (Fig. 4).

The Ge and $\mathrm{SiO_2}$ surface energy (σ_{Ge} and $\sigma_{\mathrm{SiO_2}}$, respectively) are extracted from the literature: $\sigma_{\mathrm{Ge}} \sim 700\ \mathrm{mJ/m^2}$ and $\sigma_{\mathrm{SiO_2}} \sim 600\ \mathrm{mJ/m^2}$. Since the wetting angle experimentally measured is $\sim 50°$ we find an interfacial energy $\sigma_{\mathrm{Ge\text{-}SiO_2}} \sim 150\ \mathrm{mJ/m^2}$. R and R_{FIB} are the radius of the NCs positioned on the flat surface and on the hole, respectively, R_H and h_H the radius and depth of the FIB hole.

Since the volumes of the two NCs (V_1 on the flat surface and V_2 on the hole) are equals ($V_1 = V_2$), we have

$$\frac{\pi}{3}R^3(1-\cos\theta)^2(2+\cos\theta) = \frac{\pi}{3}R_{\mathrm{FIB}}^3(1-\cos\theta)^2(2+\cos\theta) + \frac{\pi}{3}R_H^2 h_H$$

then

$$R_{\mathrm{FIB}} = \left(R^3 - \frac{R_H^2 h_H}{(1-\cos\theta)^2(2+\cos\theta)}\right)^{1/3}$$

and

$$\Delta G = \pi(\sigma_{\mathrm{Ge\text{-}SiO_2}} - \sigma_{\mathrm{SiO_2}})(\sin^2\theta(R_{\mathrm{FIB}}^2 - R^2) - R_H^2 + R_H\sqrt{R_H^2 + h_H^2}) + 2\pi\sigma_{\mathrm{Ge}}(1-\cos\theta)(R_{\mathrm{FIB}}^2 - R^2),$$

ΔG is always negative and its value depends on the geometrical features of the FIB holes and on the wetting angle.

In our experimental conditions, the experimental size of the NC measured is $\Phi_1 = 27$ nm, then its real radius and height are $R = 18$ nm and $h = 6.5$ nm and the mean volume is $V_{\mathrm{NC\text{-}exp}} = \pi h^2(R - h/3) = 2101\ \mathrm{nm}^3$. Since the volume of a conical FIB hole is $V_{\mathrm{hole}} = 1/3\ (\pi R_H^2 h_H) = 1047\ \mathrm{nm}^3$ ($h_H = 10$ nm, $R_H = 10$ nm), then $V_{\mathrm{NC\text{-}exp}} > V_H$ and when the NC is positioned on the FIB hole we have the geometrical situation described in Fig. 4. For volume conservation, the radius and the apparent size of the NCs positioned on the hole will be $R_{\mathrm{FIB}} = 14$ nm and $\Phi_2 = 21.5$ nm, respectively.

The total free energy gained when the nanocrystal nucleates inside a FIB hole with regard to when it nucleates on the flat area between the holes is $\Delta G_{\mathrm{hole\text{-}flat}} \sim -10.33$ meV/at. Therefore location of NCs inside the holes is energetically favored.

We can then conclude that ordering is mainly controlled by free energy minimization. Diffusion barrier phenomena are not considered here, but it can reasonably be assumed that they will also favor the nucleation of NCs inside the holes.[34] In particular, geometrical confinement in the holes should increase adatoms impingement and nucleation probabilities.

IV. CONCLUSION

We have investigated the crystallization of Ge nanocrystals during thermal annealing of an amorphous layer of Ge deposited on amorphous silica. We have shown that the shape of NCs is determined by the thermodynamics equilibrium shape while the density and size are only controlled by the initial deposited thickness. The evolution of mean density

and size of NCs can be fitted by $D \propto h_0^{-1}$ and $S_c \propto h_0$. The invariability of NCs morphological features with annealing temperature and time is discussed. In the second part, a preferential nucleation of Ge NCs inside the FIB holes of a prepatterned substrate has been evidenced. The driving force of NCs ordering in the holes is attributed to surface free energy minimization. Kinetically limited nucleation would also favor the nucleation inside the holes. Homogenization of NCs size is obtained for high density patterns when the interhole distance is of the same order of magnitude than the NCs size.

ACKNOWLEDGMENTS

The authors acknowledge the financial support of the EC through FORUM FIB (IST200029573).

[1] S. Tiwari, F. Rana, H. Hanafi, A. Harstein, E. F. Crabbe, and K. Chan, Appl. Phys. Lett. **68**, 1377 (1996).
[2] B. De Salvo, G. Ghibaudo, G. Pananakakis, B. Guillaumot, and T. Baron, Superlattices Microstruct. **28**, 339 (2000).
[3] Y. Liu, T. P. Chen, Y. Q. Tse, J. H. Hsieh, P. F. Ho, and Y. C. Liu, J. Phys. D: Appl. Phys. **36**, L97-L100 (2003).
[4] R. Ohba, N. Sugiyama, K. Uchida, J. Koga, and A. Toriumi, IEEE Trans. Electron Devices **49**, 1392 (2002).
[5] J. Heitmann, F. Müller, L. Yi, M. Zacharias, D. Kovalev, and F. Eichhorn, Phys. Rev. B **69**, 195309 (2004).
[6] M. Dovrat, Y. Goshen, J. Jedrzejewski, I. Balberg, and A. Sa'ar, Phys. Rev. B **69**, 155311 (2004).
[7] L. Liu, K. L. Teo, Z. X. Shen, J. S. Sun, E. H. Ong, A. V. Kolobov, and Y. Maeda, Phys. Rev. B **69**, 125333 (2004).
[8] F. Iacona, G. Franzò, and C. Spinella, J. Appl. Phys. **87**, 1295 (2000).
[9] D. Pacifici, E. C. Moreira, G. Franzó, V. Martorino, F. Priolo, and F. Iacona, Phys. Rev. B **65**, 144109 (2002).
[10] R. G. Elliman, M. J. Lederer, and B. Luther-Davies, Appl. Phys. Lett. **80**, 1325 (2002).
[11] H. E. Porteanu, E. Lifshitz, Th. Dittrich, and V. Petrova-Koch, Phys. Rev. B **60**, 15538 (1999).
[12] T. Baron, B. Pelissier, L. Perniola, F. Mazen, J. M. Hartmann, and G. Rolland, Appl. Phys. Lett. **83**, 1444 (2003).
[13] G. Hadiisavvas and P. C. Kelires, Phys. Rev. Lett. **93**, 226104 (2004).
[14] M. Luppi and S. Ossicini, Phys. Rev. B **71**, 035340 (2005).
[15] N. Daldosso, M. Luppi, S. Ossicini, E. Degoli, R. Magri, G. Dalba, P. Fornasini, R. Grisenti, F. Rocca, L. Pavesi, S. Boninelli, F. Priolo, C. Spinella, and F. Iacona, Phys. Rev. B **68**, 085327 (2003).
[16] A. R. Wilkinson and R. G. Elliman, Phys. Rev. B **68**, 155302 (2003).
[17] M. Nishida, Phys. Rev. B **70**, 113303 (2004).
[18] G. Nesher, L. Kronik, and J. R. Chelikowsky, Phys. Rev. B **71**, 035344 (2005).
[19] H.-Ch. Weissker, J. Furthmüller, and F. Bechstedt, Phys. Rev. B **67**, 245304 (2003).
[20] M. Kanoun, M. Lemiti, G. Bremond, A. Souifi, F. Bassani, and I. Berbezier, Superlattices Microstruct. **36**, 143 (2004).
[21] H. Fukuda, S. Sakuma, T. Yamada, S. Nomura, M. Nishino, T. Higuchi, and S. Ohshima, J. Appl. Phys. **90**, 3524 (2001).
[22] H. G. Yang, Y. Shi, H. M. Bu, J. Wu, B. Zhao, X. L. Yuan, B. Shen, P. Han, R. Zhang, and Y. D. Zheng, Solid-State Electron. **45**, 767 (2001).
[23] H. Omi, D. J. Bottomley, Y. Homma, and T. Ogino, Phys. Rev. B **67**, 115302 (2003).
[24] B. Yang, F. Liu, and M. G. Lagally, Phys. Rev. Lett. **92**, 025502 (2004).
[25] A. Portavoce, I. Berbezier, and A. Ronda, Phys. Rev. B **69**, 155416 (2004).
[26] M. Kawamura, N. Paul, V. Cherepanov, and B. Voigtländer, Phys. Rev. Lett. **91**, 096102 (2003).
[27] P. D. Szkutnik, A. Sgarlata, S. Nufris, N. Motta, and A. Balzarotti, Phys. Rev. B **69**, 201309(R) (2004).
[28] L. Haderbache, R. Carrigos, R. Kofman, E. Sondergard, and P. Cheyssac, Surf. Sci. **410**, L748 (1998).
[29] M. Weinberg and R. Kapral, J. Chem. Phys. **91**, 7146 (1989).
[30] M. Avrami, J. Chem. Phys. **7**, 1103 (1939); **8**, 212 (1940).
[31] V. Sessa, M. Fanfoni, and M. Tomellini, Phys. Rev. B **54**, 836 (1996); M. Fanfoni and M. Tomellini, *ibid.* **54**, 9828 (1996).
[32] B. J. Briscoe and K. P. Galvin, Phys. Rev. A **43**, 1906 (1991).
[33] Y. Wakayama, T. Tagami, and S. I. Tanaka, J. Appl. Phys. **85**, 8492 (1999).
[34] L. Nurminen, A. Kuronen, and K. Kaski, Phys. Rev. B **63**, 035407 (2000).